JOURNAL OF APPLIED ELECTROCHEMISTRY **28** (1998) 127–134

Modelling of copper etching in aerated chloride solutions

M. GEORGIADOU, R. ALKIRE

Department of Chemical Engineering, University of Illinois at Urbana-Champaign, Urbana, Illinois 61801, USA

Received 7 June 1996; revised 18 February 1997

The effect of dissolved oxygen on the rate of chemical etching of copper by acidic cuprous chloride solution was investigated numerically for the case of a rotating disc electrode (RDE). Copper dissolution in aerated acidic cupric chloride solutions of composition $3.5\,\text{M}\ CuCl_2 + 0.5\,\text{M}\ HCl + 0.5\,\text{M}\ KCl$ and $3.5\,\text{M}\ CuCl_2 + 0.5\,\text{M}\ HCl$ was investigated with consideration of the instantaneous homogeneous reaction $4\,CuCl_3^{2-} + 4H^+ + O_2 \rightleftharpoons 4\,CuCl_3^- + 2\,H_2O$ which takes place within the mass transport boundary layer. It was assumed that $CuCl_3^{2-}$ and O_2 react instantaneously, resulting in the formation of a reaction plane which separated the mass transport boundary layer into two regions: a region adjacent to the electrode where oxygen was depleted, and a region adjacent to the bulk where $CuCl_3^{2-}$ was absent. A one-dimensional mathematical model was developed to predict the position of the reaction plane. The model accounted for diffusion, migration and fluid flow generated by an RDE and included nine species and five heterogeneous electrochemical reactions. The homogeneous redox reaction served to regenerate the chemical etchant solution and thus enhance the etch rate. With increasing oxygen concentration and rotation rate the reaction plane was found to move closer toward the electrode and thus the etch rate of copper increased. Addition of KCl increased the Cl^- content in solution so as to shift the reaction plane toward the bulk.

Keywords: *copper etching*, *cuprous chloride solution*, *rotating disc electrode*, *one-dimensional model*

List of symbols

C_i	concentration of species i (mol cm^{-3})
C_{i0}	surface concentration of species i (mol cm^{-3})
$C_{i\text{ref}}$	reference concentration of species i (mol cm^{-3})
$C_{i\infty}$	bulk concentration of species i (mol cm^{-3})
C_R	characteristic concentration (0.6×10^{-3}) (mol cm^{-3})
$C_{Cl^-}^{\lambda}$	chloride ion concentration in the reference electrode compartment (mol cm^{-3})
D_i	diffusion coefficient of species i (mol cm^{2}s^{-1})
D_R	characteristic diffusion coefficient (0.72×10^{-5}) (mol cm^{2}s^{-1})
E°_{SCE}	standard potential of saturated calomel electrode (V)
E_{corr}	corrosion potential (V)
E°_j	standard potential of reaction j (V)
E^{∞}_j	equilibrium open-circuit potential of reaction j, estimated at bulk concentrations (V)
F	Faraday constant (96 484.9 C mol^{-1})
i_j	current density of reaction j (A cm^{-2})
i_{0j}	exchange current density of reaction j (A cm^{-2})
i_{0j}^{ref}	exchange current density of reaction j at reference conditions (A cm^{-2})
i_T	total net current density (A cm^{-2})
L	distance from electrode where the reaction plane is located (cm)
m	integer, 3
M_i^z	ion i participating in reaction j
n_j	number of electrons transferred in reaction j
N_i	flux of species i (mol cm^{-2}s^{-1})
p_{ij}	anodic reaction order
q_{ij}	cathodic reaction order
R	universal gas constant (J mol^{-1} K^{-1})
s_{ij}	stoichiometric coefficient of species i in reaction j
T	absolute temperature (K)
u_x	velocity normal to electrode surface (cm s^{-1})
x	direction normal to electrode surface
z_i	charge number of species i

Greek characters

α_{aj}	anodic transfer coefficient of reaction j
α_{cj}	cathodic transfer coefficient of reaction j
β	stability constant
γ_{ij}	constant exponents
δ	hydrodynamic diffusion layer thickness (cm)
η_{cj}	concentration overpotential for reaction j (V)
η_{sj}	surface overpotential for reaction j (V)
ν	kinematic viscosity (cm^2 s^{-1})
ρ_0	solvent density (kg cm^{-3})
υ_i	mobility of species i
Φ	potential in solution within the diffusion layer (V)
Φ_0	potential in solution adjacent to electrode surface (V)
ω	rotation rate (rad s^{-1})

0021-891X © 1998 Chapman & Hall

1. Introduction

Acidic cupric chloride solutions are commonly used to etch thin copper films at relatively high etch rates. The products of copper etching in these chemical systems are complexes of Cu(I) and chloride which are easily oxidized either by dissolved oxygen in aerated baths or by other oxidizing agents added to the etching solution, with the consequence that the etchant is regenerable. In this work, a mathematical model was developed to investigate the role of dissolved oxygen on the dissolution rate of copper during etching in cupric chloride solutions. The numerical technique can readily be expanded to more realistic applications of two- and three-dimensional geometries under laminar flow.

Based on previous equilibrium calculations [1], the most important Cu(II) chlorocomplexes in the system under study ($Cu/3.5\,M\ CuCl_2 + 0.5\,M\ HCl + 0.5\,M\ KCl$, in which anisotropic etching of copper was reported under certain operating conditions [1, 2] at 25 °C) are: Cu^{2+}, $CuCl^+$, $CuCl_2$ and $CuCl_3^-$. The product of all electrochemical reactions is the Cu(I) ionic complex $CuCl_3^{2-}$ which is dominant at chloride concentrations above 1 M [3]. The dissolution process is thus described by the following electrochemical reactions:

Oxidation

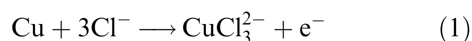

$$Cu + 3Cl^- \longrightarrow CuCl_3^{2-} + e^- \quad (1)$$

Reduction

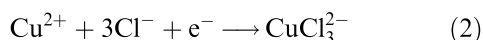

$$Cu^{2+} + 3Cl^- + e^- \longrightarrow CuCl_3^{2-} \quad (2)$$

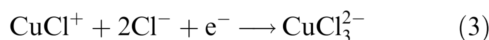

$$CuCl^+ + 2Cl^- + e^- \longrightarrow CuCl_3^{2-} \quad (3)$$

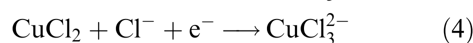

$$CuCl_2 + Cl^- + e^- \longrightarrow CuCl_3^{2-} \quad (4)$$

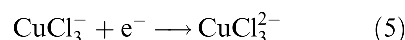

$$CuCl_3^- + e^- \longrightarrow CuCl_3^{2-} \quad (5)$$

Figure 1 illustrates the mass transport layer as well as the electrochemical reactions and the transport phenomena within the layer. The product of all electrochemical reactions ($CuCl_3^{2-}$) is transported toward the bulk and meets with incoming oxygen, which is dissolved in the solution, resulting in the following oxidation–reduction homogeneous reaction:

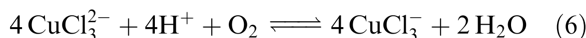

$$4\,CuCl_3^{2-} + 4H^+ + O_2 \rightleftharpoons 4\,CuCl_3^- + 2\,H_2O \quad (6)$$

The equilibrium constant for Reaction 6, calculated from free energies of formation at 298K [4], is approximately 10^{12}, a large value which in combination with the fast reaction kinetics [5] leads to the assumption that Reaction 6 occurs instantaneously at a reaction plane where the two reactants meet. The reaction plane separates the mass transport layer into two regions: (a) the region adjacent to the electrode where oxygen is absent, and (b) the region adjacent to the bulk where the cuprous species $CuCl_3^{2-}$ is depleted. At the reaction plane both $CuCl_3^{2-}$ and O_2 are totally consumed. The cupric species $CuCl_3^-$, produced at the reaction plane by the redox Reaction 6 is transported to the electrode where it reacts according to Reaction 5. Thus, the role of oxygen is to regenerate the etchant and as a consequence to enhance the rate of copper dissolution above the value that would prevail in deaerated solutions.

The formation of a reaction plane due to an instantaneous, irreversible reaction has been a subject

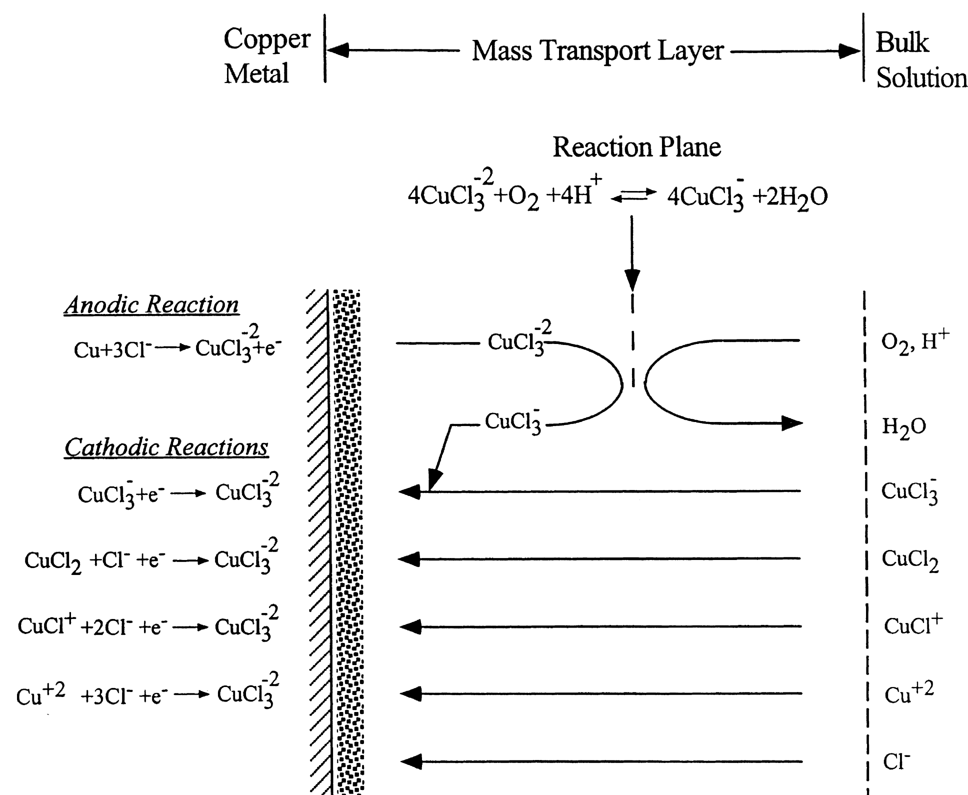

Fig. 1. Illustration of transport and reaction phenomena in the diffusion layer.

of study in simultaneous gas absorption and chemical reaction by Hatta [6], Danckwerts [7], Astarita [8] and other classic works. Acrivos [9] used the reaction plane concept to analyse laminar boundary layer flows with a homogeneous reaction. White *et al.* [10] studied the cathodic current efficiency for deposition of copper from a copper chloride solution with high levels of ferric ions by treating the formation of a reaction plane due to instantaneous reaction between cuprous chloride and ferric chloride ions.

In the present electrochemical system which involves several charged species in appreciable concentrations, the contribution of ionic migration to the total transport cannot be ignored especially within the diffusion layer. Migration is expected to affect the magnitude of the dissolution rate and the position of the reaction plane. By taking into account migration in the mathematical model, the general case for which all transport mechanisms are present is solved, and the applicability of the work is thus made more general. The purpose of the present investigation is to provide a model for aerated copper etching, which can be readily extended to realistic situations of geometry, flow field and etchant chemistry.

2. Mathematical model

2.1. *Equations and boundary conditions*

The copper rotating disk electrode (RDE) geometry was used for developing the mathematical model. Basic assumptions include steady state conditions, one dimensional domain, constant physical and transport properties, and the validity of dilute solution theory. For transport by diffusion, migration and convection, the material balance for each solute species i taking into account flow continuity was [11]

$$D_i \frac{d^2 C_i}{dx^2} + z_i F \upsilon_i \left(C_i \frac{d^2 \Phi}{dx^2} + \frac{dC_i}{dx}\frac{d\Phi}{dx} \right) - u_x \frac{dC_i}{dx} = 0 \quad (7)$$

To a very good approximation, the solution was electrically neutral

$$\sum_i z_i C_i = 0 \quad (8)$$

The reaction plane position was treated as an unknown function of position throughout the domain except at the reaction plane, a treatment similar to that used by Newman for the eigenvalues of the Graetz problem [12]:

$$\frac{dL}{dx} = 0 \quad (9)$$

The mobility υ_i was approximated by the Nernst–Einstein equation

$$\upsilon_i = \frac{D_i}{RT} \quad (10)$$

and x-velocity for the RDE system is proportional to the square of normal distance [11]:

$$u_x = -0.510\,23\ \omega \sqrt{\frac{\omega}{\nu}} x^2 \quad (11)$$

Boundary conditions were written at three boundaries: bulk, electrode surface and reaction plane.

(a) *Bulk*. At the bulk boundary, cupric chlorocomplexes and chloride ion were in equilibrium, the concentration of the product species $CuCl_3^{2-}$ was zero, and the solution potential with respect to a reference electrode placed at infinity was arbitrarily set equal to zero. The bulk concentrations also obeyed the electroneutrality condition:

$$x = m\delta = m\left(\frac{3D_R}{\alpha\nu}\right)^{1/3}\left(\frac{\nu}{\omega}\right)^{1/2} \quad (12)$$

$$C_i = C_{i\infty} \quad (13)$$

$$\Phi = 0 \quad (14)$$

Equation 9 was also written for the reaction plane position at the bulk boundary.

(b) *Electrode surface*. Each reaction was written in the general form:

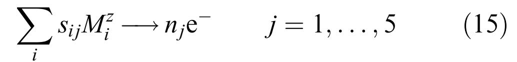

$$\sum_i s_{ij} M_i^z \longrightarrow n_j e^- \qquad j = 1, \ldots, 5 \quad (15)$$

The boundary condition for each reacting species was

$$N_i = -D_i \frac{dC_i}{dx} - z_i \upsilon_i F C_i \frac{d\Phi}{dx} = -\sum_j \frac{s_{ij} i_j}{n_j F} \qquad j = 1, \ldots, 5 \quad (16)$$

and for nonreacting species, such as H^+, K^+ and O_2,

$$N_i = -D_i \frac{dC_i}{dx} - z_i \upsilon_i F C_i \frac{d\Phi}{dx} = 0 \quad (17)$$

For the unknown potential Φ_0, a zero net current at the electrode was considered

$$i_T = \sum_j i_j = 0 \quad (18)$$

and the set of boundary conditions was completed by Equation 9 for the reaction plane position. The current density of reaction j was approximated by a Butler–Volmer equation:

$$i_j = i_{0j}\left(\exp\left(\frac{\alpha_{aj} n_j F}{RT}\eta_{sj}\right) - \exp\left(-\frac{\alpha_{cj} n_j F}{RT}\right)\right) \qquad j = 1, \ldots, 5 \quad (19)$$

The corrosion potential of the system, E_{corr}, playing the role of an overpotential for each electrochemical reaction, the concentration overpotential η_{cj} and the equilibrium potential E_j^{∞} relative to the saturated calomel reference electrode (SCE) were

$$E_{corr} - E_j^{\infty} = \eta_{sj} + \eta_{cj} \qquad j = 1, \ldots, 5 \quad (20)$$

$$\eta_{cj} = -\frac{RT}{n_j F} \ln \prod_i \left(\frac{c_{i0}}{c_{i\infty}}\right)^{s_{ij}} \qquad j = 1, \ldots, 5 \quad (21)$$

$$E_j^{\infty} = E_j^{\circ} - E_{SCE}^{\circ} - \frac{RT}{n_j F} \ln \prod_i \left(\frac{c_{i\infty}}{\rho_0}\right)^{s_{ij}} + \frac{RT}{F} \ln\left(\frac{C_{Cl^-}^{\lambda}}{\rho_0}\right) \qquad j = 1, \ldots, 5 \quad (22)$$

The derivation of the standard potential E_j° of reaction j is described in Appendix A. Substituting Equation 21 and 22 into Equation 19 and assuming that the potential Φ_0 in solution adjacent to electrode was equal to corrosion potential, the surface overpotential η_{sj} was expressed

$$\eta_{sj} = \Phi_0 - E_j^\circ + E_{\mathrm{SCE}}^\circ + \frac{RT}{n_j F}\ln\prod_i\left(\frac{c_{i0}}{\rho_0}\right)^{s_{ij}} - \frac{RT}{F}\ln\left(\frac{C_{\mathrm{Cl^-}}^{\lambda}}{\rho_0}\right) \qquad j=1,\ldots,5 \tag{23}$$

The exchange current density i_{0j} depended on concentration:

$$i_{0j} = i_{0j}^{\mathrm{ref}}\prod_i\left(\frac{C_{i0}}{C_{i\mathrm{ref}}}\right)^{\gamma_{ij}} \qquad j=1,\ldots,5 \tag{24}$$

where, for anodic reactions

$$\gamma_{ij} = p_{ij} - \alpha_{aj}\frac{s_{ij}}{n_j} \tag{25}$$

with $p_{ij} = s_{ij}$ for an anodic reactant or $p_{ij} = 0$ otherwise. For cathodic reactions:

$$\gamma_{ij} = q_{ij} + \alpha_{cj}\frac{s_{ij}}{n_j} \tag{26}$$

with $q_{ij} = -s_{ij}$ for a cathodic reactant or $q_{ij} = 0$ otherwise. Finally, for the transfer coefficients

$$\alpha_{aj} + \alpha_{cj} = n_j \tag{27}$$

(c) *Reaction plane*. $CuCl_3^{2-}$ and O_2 were instantaneously consumed as they reached the plane

$$C_{\mathrm{CuCl_3^{2-}}} = 0 \tag{28}$$

$$C_{\mathrm{O_2}} = 0 \tag{29}$$

The stoichiometry of Reaction 6 implies that

$$N_{\mathrm{O_2}}^2 + \tfrac{1}{4}N_{\mathrm{CuCl_3^{2-}}}^1 = 0 \tag{30}$$

where the superscripts 1 and 2 correspond to regions 1 and 2 of Fig. 1, respectively. The net flux of the cupric species $CuCl_3^-$ to the plane was equal to the flux of the cuprous species $CuCl_3^{2-}$, in accordance with Reaction 6, expressing an elemental copper balance:

$$N_{\mathrm{CuCl_3^-}}^2 - N_{\mathrm{CuCl_3^-}}^1 - N_{\mathrm{CuCl_3^{2-}}}^1 = 0 \tag{31}$$

A hydrogen ion balance determined the flux of H^+ to the plane

$$N_{\mathrm{H^+}}^2 - N_{\mathrm{H^+}}^1 + N_{\mathrm{CuCl_3^{2-}}}^1 = 0 \tag{32}$$

The flux of species that did not participate in Reaction 6 was continuous

$$N_i^2 - N_i^1 = 0 \quad i = \mathrm{Cu^{2+}, CuCl^+, CuCl_2, Cl^-, K^+} \tag{33}$$

In addition, the electroneutrality condition given by Equation 8 was written for the potential at the reaction plane. The values of the model parameters are provided in Tables 1, 2 and 3. The transfer coefficients α_{aj} and α_{cj} were 0.5 and the reference concentrations $C_{i\mathrm{ref}}$ were 1 M.

Table 1. Input parameters for electrochemical reactions

Reaction j	E_j^0/V	i_{0j}^{ref}/A cm^{-2}*
1	0.233	2×10^{-3}
2	0.441	3×10^{-4}
3	0.419	2×10^{-4}
4	0.431	10^{-5}
5	0.455	10^{-5}

* arbitrarily chosen.

2.2. *Method of solution*

Equations 7, 8 and 9, constrained by boundary conditions (BCs) given by Equations 13, 14, 16–18 and 28–33, constitute a highly nonlinear boundary value problem involving coupled, second order ODEs with BCs including also nonlinear, first order ODEs. A finite difference scheme was employed to solve the system numerically. Three steps were involved in the numerical solution: nondimensionalization, linearization and finite difference approximation. First the model equations and boundary conditions were made dimensionless. A Taylor series expansion was then used to linearize nonlinear terms in the equations. In the final step of finite difference approximation each of the regions shown in Fig. 1 was discretized in equally spaced intervals. Because the position of the reaction plane was unknown, the number of discrete points constituting the mesh in region 2 had to be initially guessed for a selected step size, and the step in Region 1 was unknown thus introducing additional nonlinearities. The central finite difference approximation being second order accurate with respect to the step was applied to the linearized concentration and potential equations. However, the reaction plane ODE (9), which was only used for modelling convenience, was discretized by first order accurate finite difference, forward in Region 2 and backward in Region 1. The resulting linear equation system was solved by a numerical technique developed by Newman [11]. The numerical solution proceeded from an initial guess of the solution vector which was improved by iterative solution of the equations. This

Table 2. Input parameters for species

Species	$D_i \times 10^5$ /cm^2 sec^{-1}	z_i	$C_{i\infty}\times10^3$ /mol cm^{-3}*	$C_{i\infty}\times10^3$ /mol cm^{-3}†
Cu^{2+}	0.72[20]	2	0.324	0.268
$CuCl^+$	0.72	1	1.193	1.1
$CuCl_2$	0.72	0	1.235	1.271
$CuCl_3^-$	0.72	−1	0.748	0.858
$CuCl_3^{2-}$	0.72	−2	0	0
Cl^-	2.032	−1	1.593	1.777
H^+	9.312	1	0.5	0.5
K^+	1.848[21]	1	0	0.5
O_2	1.3[22]	0	0.000 765[15]	0.000 765

* composition 3.5 M $CuCl_2$ + 0.5 M HCl.
† composition 3.5 M $CuCl_2$ + 0.5 M HCl + 0.5 M KCl.
*,† bulk concentration values determined by equilibrium calculations [1].

finite difference scheme has recently been expanded to treat more sophisticated situations of two-dimensional geometries and fluid flow, and has been implemented in anisotropic copper etching in deaerated solutions [13], and in copper deposition under conditions of high flow velocities [14], in association with more advanced nonlinear numerical solvers.

Finally, the boundary conditions at the electrode and the reaction plane boundaries were treated by the method of false boundaries [15]. At the electrode boundary an imaginary mesh point was introduced and the unknowns at this point were determined by solving together the domain equations and the boundary conditions at the electrode. At the reaction plane the treatment of the conditions was similar to that used by White [10]. Two imaginary points in either side of the reaction plane were introduced and the three sets of unknowns being the values at the reaction plane and at the two imaginary points were determined by three sets of equations being the plane conditions and the two sets of transport equations for each region applied at the plane. The electroneutrality condition completed each set of equations at the plane and the two imaginary points for the potential. Thus each region was considered as an individual computational domain and conditions were matched at the common boundary.

3. Theoretical results and discussion

The concentration profiles of all species that are present during dissolution of a copper rotating disc electrode in 3.5 M $CuCl_2$ + 0.5 M HCl + 0.5 M KCl are shown in Figs 2 and 3 for rotation rates of 100 rpm and 400 rpm, respectively. The electrode was positioned at $x = 0$. The oxygen concentration in the bulk solution was at its solubility limit [16]. It may be seen that the species that exhibited the largest change was Cl^-, which was consumed by all electrochemical reactions. The $CuCl_3^-$ species is the most thermodynamically favoured to be reduced because it has the highest reduction standard potential among all cupric chlorocomplexes (Table 1). The surface concentration of H^+ and K^+ exceed their bulk values, since these positive ions migrated towards the electrode surface during etching. The reaction plane was located at that distance from the electrode surface where the concentrations of both $CuCl_3^{2-}$ and O_2 became zero and was indicated by the dashed line.

As the rotation rate and thus fluid velocity increased, concentration changes were of course confined to a smaller region near the electrode. It may be observed in the lower portion of Fig. 3 that the slope of the concentration of product $CuCl_3^{2-}$ increased with increasing rotation rate as compared to that shown in the lower portion of Fig. 2. That is, its flux towards the reaction plane increased and the etch rate was enhanced. Such behaviour indicated a mass transfer controlled process. In addition, the reaction plane moved towards the electrode as the rotation rate increased due to convective mass transfer effects. These effects were more pronounced for O_2 rather than $CuCl_3^{2-}$ (for example a fourfold increase of the rotation rate doubled the O_2 gradient to the plane but only caused a 40% increase in the $CuCl_3^{2-}$ gradient), thus moving the reaction plane closer to the metal surface.

The effect of increasing the bulk oxygen concentration on the concentration profiles and the position of the reaction plane is illustrated in Fig. 4 for a rotation rate of 400 rpm. Comparison between Figs 4 and 3 reveals that the homogeneous reaction took place nearer the electrode when the oxygen level was increased, and that the gradient of $CuCl_3^{2-}$ to the plane was higher (see the lower portions of Figs 4 and 3). As a result, the etch rate is expected to be higher. The dependence of the location of the reac-

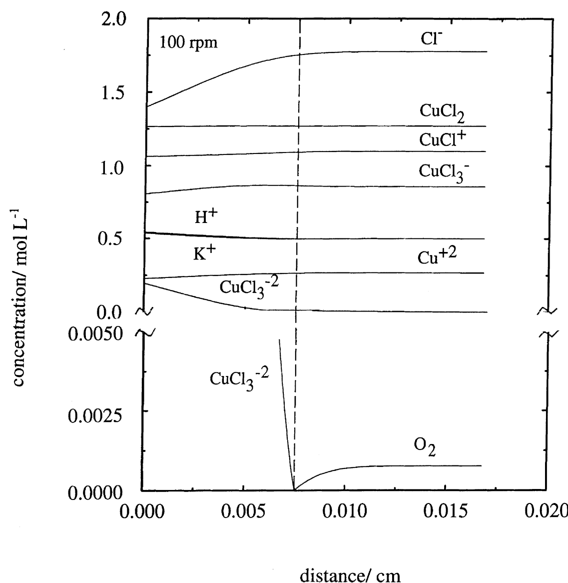

Fig. 2. Concentration profiles of all species and detail for O_2 at 100 rpm and 0.000 765 M O_2 (solubility limit); Cu/3.5 M $CuCl_2$ + 0.5 M HCl + 0.5 M KCl.

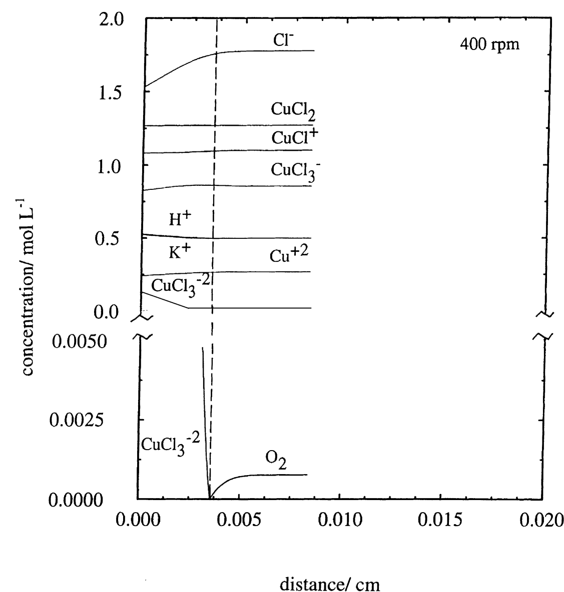

Fig. 3. Concentration profiles of all species and detail for O_2 at 400 rpm and 0.000 765 M O_2 (solubility limit); Cu/3.5 M $CuCl_2$ + 0.5 M HCl + 0.5 M KCl.

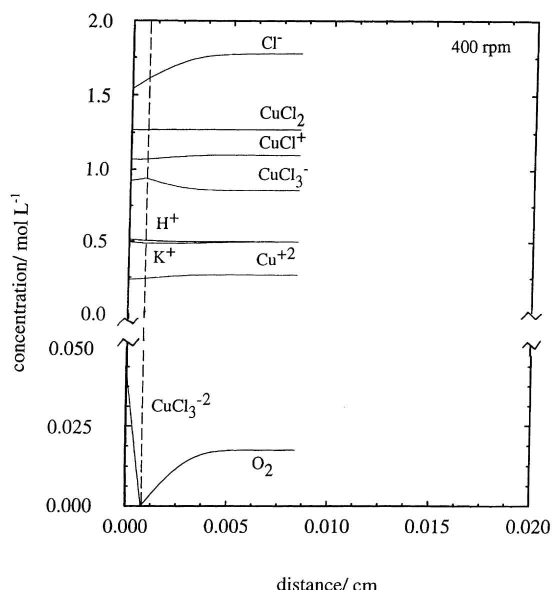

Fig. 4. Concentration profiles of all species and detail for O_2 at 400 rpm and 0.0174 M O_2; Cu/3.5 M $CuCl_2$ + 0.5 M HCl + 0.5 M KCl.

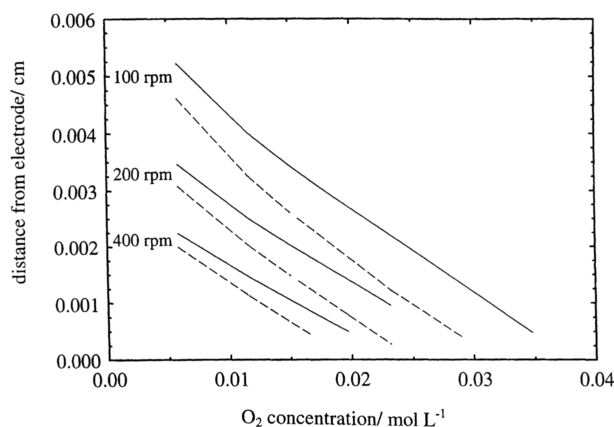

Fig. 5. Variation of reaction plane position with O_2 concentration and rotation rate: 3.5 M $CuCl_2$ + 0.5 M HCl + 0.5 M KCl (solid curves) and 3.5 M $CuCl_2$ + 0.5 M HCl (dashed curves).

tion plane on the bulk concentration of oxygen is clearly seen in Fig. 5 for the 3.5 M $CuCl_2$ + 0.5 M HCl + 0.5 M KCl (solid curves) and the 3.5M $CuCl_2$ + 0.5 MHCl (dashed curves) solutions, respectively, at various rotation rates. This dependence was almost linear for all rotation rates. The reaction plane was closer to the electrode for higher oxygen bulk concentrations due to the diffusion mass transfer effect, and also for higher fluid velocities due to the convective mass transfer effect on the equilibrium of the regeneration reaction. Furthermore, comparison between the solid and the dashed curves of Fig. 5 leads to the conclusion that the reaction occurred nearer to the metal surface at all flow rates for the case of the solution with the less chloride content (i.e., 3.5 M $CuCl_2$ + 0.5 M HCl), due to the fact that equilibrium was satisfied at smaller oxygen concentrations in the lower chloride concentration. The behaviour shown in Fig. 5 as arising from excess chloride content may as well be attributed to migration effects. The migration of the reacting chloride ion towards local anodes is increased in the solution with higher chloride content (i.e., 3.5 M $CuCl_2$ + 0.5 M HCl + 0.5 M KCl) resulting in higher production rates of the dissolution product $CuCl_3^{2-}$; consequently, the mass transfer rate of this species toward the bulk would be higher and the regeneration reaction would occur at a greater distance from the electrode surface.

4. Conclusions

It was concluded that the position of the reaction plane where regeneration reaction of etching solution occurs was driven closer to the metal surface when oxygen concentration and rotation rate increased. In contrast, the influence of higher chloride concentration was to move the reaction plane farther from the electrode as a result of increased migration contribution of the chloride reacting ion. All these effects were attributed to the instantaneous equilibrium of the regeneration reaction which was automatically satisfied at such a location within the diffusion layer where the necessary requirements in reactant concentrations were met. The impact of regeneration was to enhance the etch rate relative to the deaerated case; besides the rate was increased by convection, and by an increase of chloride content.

It should be mentioned here that when the oxygen levels were at the saturation limits in the bulk solution, the regeneration of the etching solution via the redox reaction took place almost at the edge of the diffusion layer to the bulk. By increasing oxygen activity over the solubility limit such as by addition of more aggressive oxidizing agents, regeneration very close to the metal surface would be obtained, under which conditions the enhancement of the etch rate would become considerable.

The one-dimensional calculations described in this work can be readily expanded to more complicated two and three-dimensional geometries where the flow fields are complex (for example rectangular cavities) and can thus be used to make qualitative predictions

Table 3. Values for exponents γ_{ij}

Reaction	Cu^{2+}	$CuCl^+$	$CuCl_2$	$CuCl_3^-$	$CuCl_3^{2-}$	Cl^-
1	0	0	0	0	α_{a1}	$3(1-\alpha_{a1})$
2	$1-\alpha_{c2}$	0	0	0	α_{c2}	$3(1-\alpha_{c2})$
3	0	$1-\alpha_{c3}$	0	0	α_{c3}	$2(1-\alpha_{c3})$
4	0	0	$1-\alpha_{c4}$	0	α_{c4}	$1-\alpha_{c4}$
5	0	0	0	$1-\alpha_{c5}$	α_{c5}	0

for the local dissolution rate along the metal surface. For regions of the surface that are exposed to high fluid velocities it could be anticipated that regeneration of the etching solution would take place almost on the surface, and therefore the etch rate would be enhanced. On the other hand, for those parts of the surface that are exposed to very low flow velocities, the regeneration reaction would occur farther from the surface, and thus the etch rate would be anticipated to be much lower. The distribution of etch rate along the metal surface would thus be nonuniform in a way that involves the surface geometry, the flow field, and the etchant chemistry.

References

[1] M. Georgiadou and R. C. Alkire, *J. Electrochem. Soc.* **140** (1993) 1340.

[2] *Idem, ibid.* **140** (1993) 1348.

[3] H. P. Lee and K. Nobe, *ibid.* **133** (1986) 2035.

[4] D. D. Wagman, W. H. Evans, V. B. Parker, I. Halow, S. M. Bailey and R. H. Schumm, National Bureau of Standards, Technical Notes (1968) 270–273 and (1969) 270–274.

[5] F. Hine, K. Yamakawa, *Electrochim. Acta* **15** (1970) 769.

[6] S. Hatta, *Techn. Rep. Tohoku Imp. Univ.* **8** (1928) 1.

[7] P. V. Danckwerts, 'Gas–Liquid Reactions', McGraw-Hill, New York (1970).

[8] G. Astarita, 'Mass Transfer with Chemical Reaction', Elsevier, Amsterdam (1967).

[9] A. Acrivos, *Chem. Engng Sci.* **13** (1960) 57.

[10] R. White, J. A. Trainham, J. Newman and T. W. Chapman, *J. Electrochem. Soc.* **124** (1977) 669.

[11] J. S. Newman, 'Electrochemical Systems', Prentice-Hall, Englewood Cliffs, NJ (1973).

[12] J. Newman, *Electroanal. Chem.* **6** (1973) 187.

[13] M. Georgiadou and R. C. Alkire, *J. Electrochem. Soc.* **141** (1994) 679.

[14] M. Georgiadou, 189th Electrochemical Society Meeting, Los Angeles, 5–10 May (1996).

[15] M. E. Davis, 'Numerical Methods and Modeling for Chemical Engineers', J. Wiley & Sons, New York (1984).

[16] A. S. Jhaveri and M. M. Sharma, *Chem. Engng Sci.* **22** (1967) 1.

[17] R. W. Ramette, *Inorg. Chem.* **25** (1986) 2481.

[18] L. S. Sillen, A. E. Martell, 'Stability Constants of Metal-Ion Complexes', The Chemical Society, Burlington House, London W1, Special Publication no. 17 (1964).

[19] W. M. Latimer, 'The Oxidation States of the Elements and Their Potentials in Aqueous Solutions', 2nd edn, Prentice-Hall, New York (1952).

[20] T. V. Nguyen, C. W. Walton, R. E. White and J. Van Zee, *J. Electrochem. Soc.* **133** (1986) 81.

[21] T. W. Chapman and J. Newman, 'A Compilation of Selected Thermodynamic and Transport Properties of Binary Electrolytes in Aqueous Solution', University of California, Publ. no. UCRL-17767 (1968).

[22] C. G. Law, Jr and J. Newman, *J. Electrochem. Soc.* **133** (1986) 37.

Appendix A

Standard potentials. The formulas for the standard potentials of Reactions 1–5, which are not tabulated in reference books because they involve complexation with chloride, are

$$FE^\circ_{Cu/CuCl_3^{2-}} = FE^\circ_{Cu/Cu^+} - RT\ \ln\ \beta_{cuprous} \quad (A.1)$$

$$FE^\circ_{CuCl_3^{2-}/Cu^{2+}} = FE^\circ_{Cu^+/Cu^{2+}} + RT\ \ln\ \beta_{cuprous} \quad (A.2)$$

$$FE^\circ_{CuCl_3^{2-}/CuCl^+} = FE^\circ_{Cu^+/Cu^{2+}} + RT\ \ln\ \frac{\beta_{cuprous}}{\beta_1} \quad (A.3)$$

$$FE^\circ_{CuCl_3^{2-}/CuCl_2} = FE^\circ_{Cu^+/Cu^{2+}} + RT\ \ln\ \frac{\beta_{cuprous}}{\beta_2} \quad (A.4)$$

$$FE^\circ_{CuCl_3^{2-}/CuCl_3^-} = FE^\circ_{Cu^+/Cu^{2+}} + RT\ \ln\ \frac{\beta_{cuprous}}{\beta_3} \quad (A.5)$$

$\beta_{cuprous}$, β_1, β_2 and β_3 are stability constants of $CuCl_3^{2-}$, $CuCl^+$, $CuCl_2$ and $CuCl_3^-$ formation reactions:

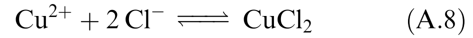

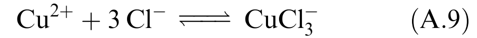

Based on equilibrium constants of the successive equilibrium reactions [17], the stability constants for Reactions A.7–A.9 were calculated: $\beta_1 = 2.31$, $\beta_2 = 1.5015$ and $\beta_3 = 0.570\,57$. The stability constant for Reaction A.6 was obtained directly from literature [18]: $\beta_{cuprous} = 11.21$. The standard potentials for oxidation of metallic copper to cuprous ion and of cuprous to cupric ion are 0.521 and 0.153 V vs NHE [19]. With this information the standard potentials of Reactions 1–5 were calculated by Equations A.1–A.5 and their values are listed in Table 1.

Current densities. For notational convenience the unknowns were numbered: (1) Cu^{2+}; (2) $CuCl^+$; (3) $CuCl_2$; (4) $CuCl_3^-$; (5) $CuCl_3^{2-}$; (6) Cl^-; (7) H^+; (8) K^+; (9) O_2; (10) Φ; (11) L. The values of constant exponents γ_{ij} summarized in Table 3 were calculated by Equations 25–26 and substituted into Equation 24 to obtain the analytical expression for the exchange current density. Substituting the latter and the surface overpotential Equation 23 into Equation 19, the current density was derived in terms of surface concentrations and potential for the oxidation and reduction reactions 1–5. Therefore, for oxidation:

$$i_1 = i_{01}^{ref}\left[\left(\frac{C_{60}}{C_{6ref}}\right)^3 \exp\left(\frac{\alpha_{a1}F}{RT}(\Phi_0 - U_1)\right) - \left(\frac{C_{50}}{C_{5ref}}\right)\exp\left(-\frac{\alpha_{c1}F}{RT}(\Phi_0 - U_1)\right)\right] \quad (A.10)$$

and for reduction (A.11):

$$i_j = i_{0j}^{\mathrm{ref}} \left[\frac{C_{50}}{C_{5\mathrm{ref}}} \exp\left(\frac{\alpha_{aj} F}{RT} (\Phi_0 - U_j) \right) - \frac{C_{j-1,0}}{C_{j-1,\mathrm{ref}}} \left(\frac{C_{60}}{C_{6\mathrm{ref}}} \right)^{|s_{6,j}|} \times \exp\left(-\frac{\alpha_{cj} F}{RT} (\Phi_0 - U_j) \right) \right]$$

for $j = 2, \ldots, 5$, and where

$$U_1 = E_1^\circ - E_{\mathrm{SCE}}^\circ - \frac{RT}{F} \ln\left(\frac{C_{6\mathrm{ref}}^3}{C_{5\mathrm{ref}} \rho_0^2} \right) + \frac{RT}{F} \ln\left(\frac{C_{\mathrm{Cl}^-}^\lambda}{\rho_0} \right)$$

$$U_j = E_j^\circ - E_{\mathrm{SCE}}^\circ + \frac{RT}{F} \ln \frac{C_{j-1,\mathrm{ref}}}{C_{5\mathrm{ref}}} \left(\frac{C_{6\mathrm{ref}}}{\rho_0} \right)^{|s_{6,j}|} + \frac{RT}{F} \ln\left(\frac{C_{\mathrm{Cl}^-}^\lambda}{\rho_0} \right) \quad (A.13)$$